PCCP

Accepted Manuscript

ROYAL SOCIETY OF CHEMISTRY

www.rsc.org/pccp

Challenges of Modelling Real Nanoparticles: Ni@Pt Electrocatalysts for the Oxygen Reduction Reaction

G. Ramos-Sanchez[1,2], S. Praserthdam[1], F. Godinez-Salomon[3], C. Barker[1], M. Moerbe[1], H.A. Calderon[4], L.A. Lartundo[5], M.A. Leyva,[3] O.Solorza-Feria[3], and P.B. Balbuena[1]

1. Department of Chemical Engineering, Texas A&M University, College Station, Texas 77843, USA
2. Universidad Autónoma Metropolitana - Iztapalapa, Departamento de Química, 55-534, C.P. 09340 México, D.F., México.
3. Departamento de Química, Centro de Investigación y de Estudios Avanzados del IPN, A. Postal 14-740, C.P. 07360, México D.F., México.
4. Depto. de Ciencia de Materiales, ESFM-IPN, Zacatenco México-D.F. CP. 07738, México.
5. Centro de Nanociencias y Micro y Nanotecnologías-IPN, UPALM, Zacatenco México-D.F. CP. 07738, México.

Submitted to PCCP themed issue on Recent Advances in the Chemical Physics of Nanoalloys,

Revision submitted April 1, 2015

Abstract

Theoretical/computational methods have been extensively applied to screen possible nano-structures attempting to maximize catalytic and stability properties for applications in electrochemical devices. This work shows that the method used to model core@shell structures is of fundamental importance in order to truly represent the physicochemical changes arising from the formation of a core-shell structure. We demonstrate that using a slab approach for modelling nanoparticles the oxygen adsorption energies are qualitatively well represented. Although this is a good descriptor for the catalytic activity, huge differences are found for the calculated surface stability between the results of a nano-cluster and those of a slab approach. Moreover, for the slab method depending on the geometric properties of the core and their similarity to the elements of the core or shell, contradictory effects are obtained. In order to determine the changes occurring as the number of layers and nano particle size are increased, clusters of Ni@Pt from 13 to 260 atoms were constructed and analyzed in terms of geometric parameters, oxygen adsorption, and dissolution potential shift. It is shown that the results of modelling the Ni@Pt nanoparticles with a cluster approach are in good agreement with experimental geometrical parameters, catalytic activity, and stability of a carefully prepared series of Ni@Pt nanostructures where the shell thickness is systematically changed. The maximum catalytic activity and stability are found for a monolayer of Pt whereas adding a second and third layer the behavior is almost the same than that in pure Pt nanoparticles.

Introduction

The implementation of a hydrogen economy based on generation/transformation of hydrogen using electrochemical devices is one of the best options to replace today's fossil economy which uses the polluting fuel combustion to generate energy [1,2]. The economic viability of the hydrogen economy relies on the development of more active materials to be used in Polymer Electrolyte Membrane (PEM) electrolyzers to generate hydrogen [3,4] and fuel cells (FC) to transform it into energy [5,6]. Up to now, a high number of new structures, compounds and alloys have been proposed to substitute the scarce and expensive platinum

catalyst. Among them, core-shell structures with a less noble metal as core and platinum shell have the advantage of a high utilization of Pt and the modification of its electronic structure by the influence of the core either by a geometric or ligand effect [7-14]. As a result, the catalytic activity of the catalysts is enhanced, especially for the sluggish oxygen reduction reaction (ORR) during PEMFC operation. Despite the accumulated knowledge regarding these materials, still unresolved issues remain on the effect of the core on the surface reactivity, such as determining the number of layers that maximize the catalytic activity and durability.

In addition to the required high catalytic activity for the ORR, the durability of the nanoparticles is of extreme concern. A number of chemical changes can occur during oxygen adsorption and subsequent electron transfer steps of the ORR that could lead to the destruction of the original catalytic structure. Among them, the dissolution of surface atoms, segregation of less noble metals from the core to the surface, and re-deposition of other metals on the surface are crucial[15,16]. Therefore the search for new materials with the desired properties for applications in PEMFCs is an important activity with a milliard of possible geometries, components, compositions, and size. In order to screen many possible candidates for both enhanced catalytic activity and durability, computational methods have been widely used especially those based on the density functional theory (DFT)[17-19].

The slab approach is one of the most commonly used methods to model nanoparticles. This method has been widely used to determine changes in surface reactivity as function of composition, concentration, and geometry[7,20-23]. From a practical point of view, the simulation cell consists of a solid slab with a vacuum space; the cell is then repeated periodically in three directions. The slab intends to represent the bulk surface; the atoms of the bottom layers are kept fixed to represent the bulk behavior of the solid while those of the near surface layers are allowed to move. This approach is very useful to represent pure solid surfaces, as well as pure and alloyed large nanoparticle surfaces. Another advantage is the possibility of studying many possible structures and compositions in a systematic way. However, there is no implementation on available academic or commercial software of non-orthorhombic periodic systems; therefore, the relaxation of the interface when two different systems interact has been impossible to represent and usually one has to constrain one system to the structure of the other. In consequence, using slab models to represent small core-shell, skin layers, and alloy nanoparticles the question of whether the lattice parameters of the solid represent correctly or not the geometric properties of the nanoparticle core is a debatable topic, i.e. will the outermost layers remain strained to the parameters of the core while the core remains unchanged? On the other hand, modelling nanoparticles with a cluster approach does not have any geometric constrain but the computational requirements to model a real nanoparticle is many times out of the available capacities. Therefore, this method is limited to study a few atoms and a very small number of possible candidates[24-26]. Both approaches are mere representations of a real nanoparticle, the question of whether the slab or the small clusters better represent a real nanoparticle is of primordial importance since designing new materials by computational methods requires that the model used to represent nanoparticles is capable of evaluating correctly the properties under analysis.

Despite that Ni@Pt core-shell nanoparticles have been proposed some years ago as good alternatives to replace pure Pt nanoparticles in order to enhance the ORR kinetics, their physical properties and catalytic behavior are not yet well understood. Previous theoretical analysis of the activity and stability of core-shell and Pt-skin on a Ni core have used the slab approach with the Ni structural parameters to represent the core[27,28]. By using this method the catalytic activity was predicted to be better than that of platinum;

however, the stability is predicted to be poor owed to the excess strain induced by the Ni core [28]. One of the reasons behind the use of alternative alloys of PdNi and PtNi as core is that in this case the strain of the shell is less extreme[29-31].

In this paper we use a combined theoretical/experimental approach aiming to investigate the factors that affect both the reactivity and stability of Ni@Pt nanoparticles. We focus on the fundamental question of the correctness of the slab models generally used to represent nanoparticles, and how the activity and stability properties would compare with those calculated by a cluster approach. In addition, we are interested in determining the number of shells needed to enhance the catalytic activity and what is their effect on the particle surface stability.

Computational Details

The Vienna Ab Initio Software Package (VASP)[32,33] was used for all the spin polarized DFT calculations. Basis functions were constructed using the Projector Augmented Wave (PAW) method for the valence electrons [34] along with the Revised Perdew-Burke-Ernzerhof (RPBE) exchange-correlation functional[35]. In all cases the plane-wave cutoff energy was optimized and set equal to 400 eV, and the total energy was calculated using the Methfessel-Paxton of first order with a 0.2 eV gaussian smearing for the partial occupancies. The irreducible Brillouin zone was sampled with a Monkhorst-Pack grid of 11x11x1 and 1x1x1 for slabs and clusters calculations respectively. Ground state energies and charge densities were calculated self-consistently using the blocked Davidson minimization algorithm by minimizing the Hellman-Feynman forces. For slab calculations the Ni or Pt lattice parameters were used to construct the cell as explained later, different number of layers were used to represent the core-shell structures. For cluster calculations it was ensured that the cell was large enough (28 Å) to avoid self-interactions for the largest cluster (the same cell was used in all cases). For all cases the convergence criteria was set to 10^{-4} and 10^{-3} eV/cell for successive electronic and ionic steps respectively.

Experimental Procedure

Synthesis of electrocatalysts. $Ni_x@Pt_{100-x}$ catalysts supported on functionalized carbon Vulcan, with different nominal atomic ratios and a target metal loading of 30 wt% were prepared in two steps, following a modified procedure based on a previous report[36]. In a first step, Ni-core nanoparticles were prepared by mixing $Ni(NO_3)_2.6H_2O$ (5.625 g, 19.34 mmol) and tetrabutyl ammonium bromide (TBAB) (4.98 g, 15.45 mmol) in 150 mL of ethanol. The solution was transferred and magnetically stirred for 4 h in a homemade reactor adapted with an ultrasonic probe and cooling jacket. Then, keeping the N_2 atmosphere and 283 K, the reduction was carried out slowly adding a fresh solution of $NaBH_4$ (4.3 g, 116 mmol) in 50 mL of ethanol. In this stage, ultrasonic probe was switch on/off every 10 s. After complete addition of reducing agent, the reaction continued for 30 min. A black powder (Ni-Core), was obtained by centrifugation, then copiously washed with MQ-Water (18.2 MΩ) and finally with ethanol. Core-shell nanoparticles were prepared by dispersing the as-prepared Ni nanoparticles (254 mg, 4.32×10^{-3} mol) and adding TBA (1.3951 g, 4.32×10^{-3} mol) in 100 mL of water, the slurry was magnetically agitated during 2 h. Then, varying amounts of a solution of $H_2PtCl_6.6H_2O$ in water were added drop stepped manner over a period of 30 min. The powder was then dried in N_2 atmosphere at 413 K during 1 h. The bulk composition was determined by energy dispersive spectroscopy (EDS) which showed the average residual composition of 18, 38, 44 and 70 wt. % of Pt respect to Ni-core, hereafter labeled as: $Ni_{82}@Pt_{18}$, $Ni_{62}@Pt_{38}$, $Ni_{56}@Pt_{44}$ and $Ni_{30}@Pt_{70}$.

Electrochemical characterization. The electrochemical measurements were conducted at constant temperature (278 K), in a typical three-electrode cell, using a rotating disk electrode (RDE) setup and potenciostat/galvanostat (PARSTAT model 2273). A Pt mesh and a freshly prepared reversible hydrogen electrode (RHE) were used as counter and reference electrode respectively. A glassy carbon used as working electrode (0.196 cm^2), was prepared considering previous reports [37]. A Pt loading previously optimized of 16 μgPt cm^{-2} was used. The working electrode was immersed under potential control at 0.1 V in nitrogen-saturated 0.1 M $HClO_4$, the potential was then cycled 30 times between 0.05 V and 1.2 V, in order to obtain a reproducible voltammogram. The ORR was carried out in an oxygen-saturated electrolyte. IR-compensation and background subtraction, using a CV in N_2-saturated electrolyte, were considered to obtain electrochemical parameters. The electrochemical surface area was calculated by CO-stripping, considering 420 μC cm^{-2} as the charge of a monolayer. The results were compared with that of a commercial Pt/C (Etek) catalyst.

X-ray Photoelectron Spectroscopy (XPS). XPS measurements were performed with a Thermo Scientific K-alpha spectrometer using monochromatic radiation Al Kα source (1487 eV). Instrument base pressure was $1x10^{-9}$ mBar. The High-Resolution spectra of the target elements (Pt 4f and Ni 2p) were collected using an analysis area of 400 μm^2 at pass energy of 60 eV, with a resolution of 0.6 eV. The signal of C1s (248.5 eV) was considered as reference to correct charging effects. The quantitative analysis was carried out using average spectra collected from different sample regions. The data were analyzed using AD-VANTAGE software (v5.932). Smart-Shirley baseline and Gaussian (Y%)-Lorentziant (X%) profile were used for each component.

X-ray Diffraction (XRD). XRD patterns were collected in a diffractometer Bucker D2-Phaser using Cu-Kα (1.5418 Å) and a linear Lyxeye detector. The Rietveld refinement was carried out using TOPAS academic v. 3.0.

Results and Discussion

In order to determine the changes that a pure Ni core has on the Pt shell as a function of the number of layers we performed two types of slab simulations. In the first type, the lattice parameters (LP) of Ni were used to construct the slab, therefore the Pt shell is always strained to the LP of Ni (Ni LP). In the second type we used the Pt LPs to build the slab, the Ni core is kept at the Pt LP; therefore, the Pt shell is not strained but the Ni core is. It is expected that the experimentally obtained nanoparticle will have an intermediate behavior; so we intend to determine which of the two slab approaches is more adequate to represent the system. All the slab simulations were performed with six-layers; therefore, for a pure Pt system six layers of Pt were used, for pure Ni, six layers of Ni, for Pt:Ni (1:1), the system contains 3 Pt layers and 3 Ni layers and so on.

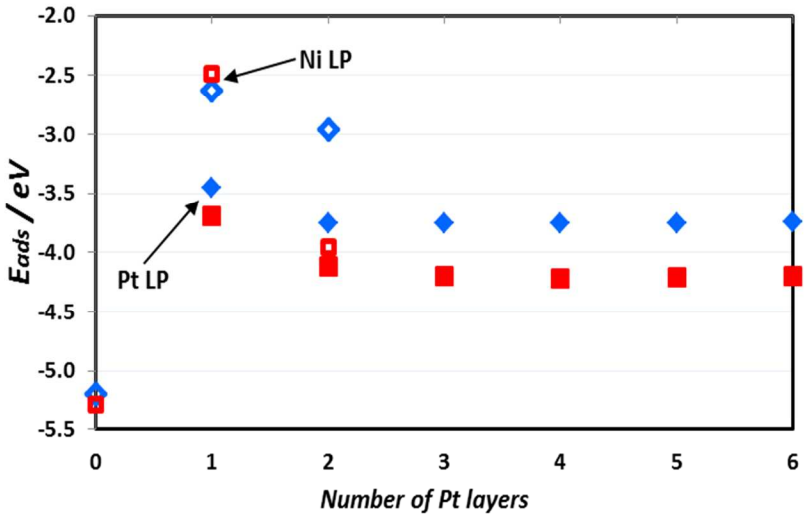

Figure 1. Oxygen adsorption energy on Ni@Pt systems with varying number of Pt layers on the shell modeled with the slab approach. Close and open symbols correspond to Pt LP and Ni LP respectively. Adsorption on fcc and hcp sites is depicted as square red and rhombic blue symbols respectively.

It has been reported that the oxygen adsorption energy (E_{ads}) (and adsorption of intermediates) is a good descriptor of the catalytic activity. If the adsorption is too strong, the removal of subproducts (especially OH) is very difficult, if the adsorption is too weak, electron transfer from the electrode becomes very difficult[38]. Platinum, the most widely used electrocatalyst, adsorbs oxygen a little bit strongly; therefore finding better catalysts is devoted to search for materials that adsorb oxygen weaker (~ 0.2 eV according to a kinetic model [39]). Figure 1 depicts the calculated changes in the oxygen adsorption energy as the number of layers of platinum in the shell changes: a single O atom was added close to the specific site and then optimized. Seminal papers have analyzed the oxygen adsorption on metal surfaces.[18,40-42] To simplify the analysis we will focus on O adsorption on fcc sites (square red symbols in Figure 1) since the trends are similar than in hcp sites (blue symbols in Figure 1). The adsorption energy on pure Pt (6 layers slab) reproduces very well previous calculated results[26,43]; on the other hand, the adsorption on pure Ni (0 Pt layers) is about 1 eV stronger than in Pt which implies poor ORR electrocatalytic activity of Ni nanoparticles. For five, four, and three layers of Pt on Ni core with Pt LP is obtained the same oxygen adsorption energy as on pure Pt i.e. the Ni core does not have an effect on the catalytic properties of the surface. On the other hand, for the system with Ni LP having five, four, and three layers of Pt, the Pt layers become separated from the Ni core as soon as oxygen is added to the system. Therefore, the effect of the core is also nullified (no data shown in Figure 1). Since these slabs are approximations to the nanoparticle structure, we conclude that in a nanoparticle one or two layers of Pt can be accommodated over the Ni core. In contrast, for more than two Pt layers the situation could be more complex, especially in presence of the electrolyte and acidic conditions on fuel cell environments. However, from a very simple perspective, two different processes can occur: 1) the Pt shell layers remain constrained to the geometric structure of Ni, and the stability of the system becomes poorer so the shell components may tend to separate from the core forming separated Pt nanoparticles, or 2) the system allows more atoms of Pt in the shell in order to avoid the straining by forming dislocations. In the latter case the catalytic properties will not be

affected by the core beyond the third layer of Pt but surely will be affected by the presence and nature of the dislocations. Ignoring the effect of the dislocations, more than two layers of Platinum on the Ni core either on Pt or Ni LP core do not have an effect on the catalytic activity of the system.

For a Pt monolayer on the Ni core the effect on the oxygen adsorption is maximized (Figure 1): the weakest adsorption energy is found. Two different results are observed depending on the stress imposed to the surface layer. For the Pt monolayer strained to the Ni LP the adsorption energy is about ~1.5 eV weaker than that in Pt while in the non-strained layer the decrease is only ~0.5 eV. The energy difference between the two systems can be rationalized by the fact that the strained system has two components: 1) the ligand effect caused by the presence of Ni and also 2) the strain effect caused for the different Pt-Pt distance on the surface layer. On the contrary, only the ligand effect of Ni is present on the non-strained system. For 2-layers of Pt there is a very small effect from the core only on the non-strained system while on the strained one the effect depends on the site of adsorption of oxygen: on the hcp site the surface reconstructs while on the fcc it does not. This is a first indication that even with two layers of Pt the strained system is very unstable; therefore the real system might be far from the strained conditions here imposed.

In order to explore the influence of Ni-Pt ratio over the catalytic activity for the ORR on $Ni_x@Pt_{100-x}/C$ nanoparticles, a series of Ni@Pt nanoparticles were prepared. The size of the core is the same while increasing quantities of Pt are used to form thicker shells. As shown in Figure 2, the onset potential for the ORR is shifted positively for all $Ni_x@Pt_{100-x}/C$ catalysts in comparison with commercial Pt/C. Overall, the specific activity (SA) at 0.9 V, expressed as current density after specific surface area normalization, showed improvement factors around 3-6 times with respect to that of Pt/C. The results showed that a Ni:Pt ratio with 18 wt. % of Pt in the $Ni_x@Pt_{100-x}/C$ leads to the most active catalysts. Lower enhancement was observed for those with higher Pt amount. These results are consistent with those reported by C. Wang et al. [29], who found optimum activity performance with one or two monolayers of Pt deposited onto a Pt-Ni substrate, whereas this performance decreases when the number of Pt layers increases. On the other hand, mass activity (MA) was not observed to be as favored as in the case of SA. Only the catalysts $Ni_{82}@Pt_{18}/C$ maintained performance higher than the commercial one.

The electrochemical results indicate better catalytic activity for lower amounts of shell components; however, the specific structure of the samples may evolve differently under the electrochemical conditions to that assumed during syynthesis. Thus, to verify details of the structure, quantitative chemical state information from Ni-core and core-shell catalysts ($Ni_x@Pt_{100-x}$) was obtained by XPS. For clarity, only spectra of Ni $2p_{3/2}$ and Pt $4f_{7/2}$ from Ni-core and $Ni_{82}@Pt_{18}$ catalysts are shown in Figure 3 a-b, however the values from all catalysts here evaluated are summarized in Supplementary Information, Table S1. The Ni 2p spectra exhibited complex multiplet splitting, related with a multi-electronic excitation[44]. The Ni-core material showed both metallic and oxide contribution peaks at the binding energies of 852.4 and 853.8 eV respectively. The presence of NiO on the core was confirmed by Atomic Resolution Electron Microscopy: two types of particles were found, the largest ones corresponding to pure Ni and a low amount of small ones composed of NiO (Supplementary information Figure S1). Figure 3b shows the XPS profile for $Ni_{82}@Pt_{18}$ (left) and the quantitative analysis of normalized Ni and Pt content for the Ni-core and $Ni_x@Pt_{100-x}$ catalysts (right). The quantitative analysis showed an increase of Pt content as envisaged in the synthesis. However, while the change in composition for the lowest amount of Pt is important, evident, and very close to that obtained by EDS, increasing the amount of Pt the concentration seems to double that of the sample with lowest amount of Pt; moreover, the value does not change with higher

amounts of Pt. Different studies have determined that the formation of Pt monolayers is possible by dissolution of Ni and Pt segregation to the surface on the acidic and oxidizing conditions present on hydrogen fuel cells [45-48]; therefore, it is mostly probable that the lowest content of Pt on the core-shell suggests the formation of a monolayer of Pt while for the higher amounts of Pt the formation of the same multilayer (probably two or three monolayers) of Pt. The presence of NiO surely has an effect on both the catalytic and stability properties in case that Pt also deposits on NiO; however, a model including both types of nanoparticles is out of the scope of this work. Besides the Ni and NiO nanoparticles are well separated indicating that the effect explained on this paper on Ni@Pt is still valid while further clarification needs to be performed on NiO nanoparticles.

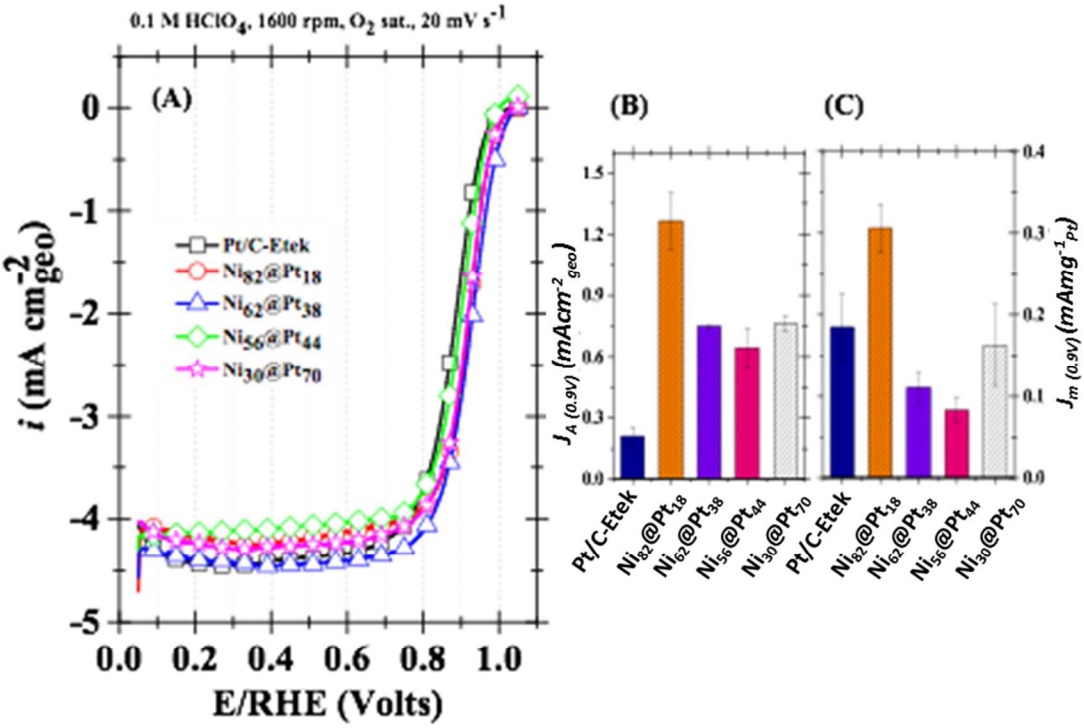

Figure 2. Electrochemical study of $Ni_x@Pt_{100-x}/C$ by RDE. Potentiodynamic curves at 1600 rpm into O_2 saturated electrolyte 0.1 M $HClO_4$, after background line subtraction (A). Summary of specific and mass activities respectively, (B) and (C).

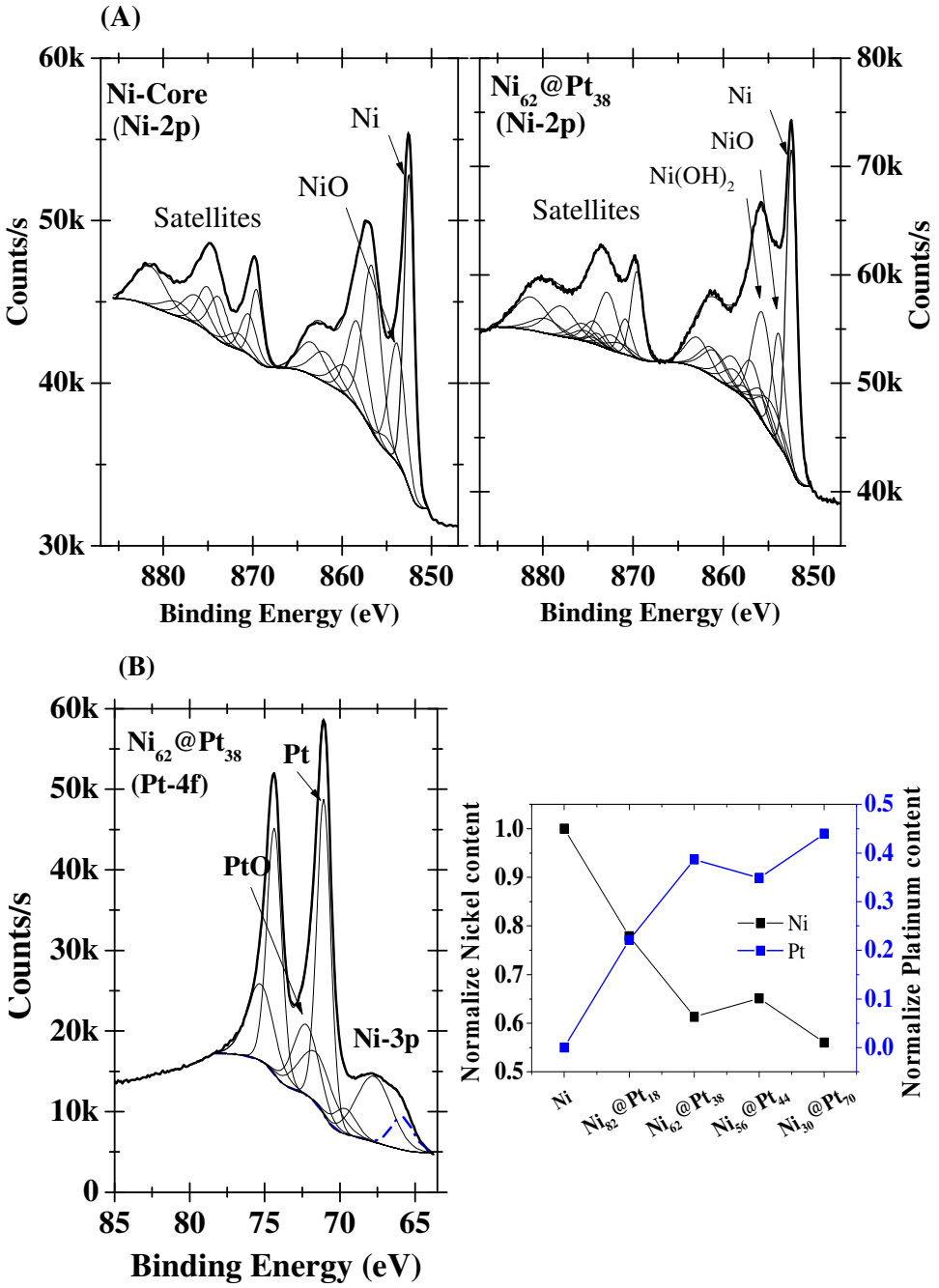

Figure 3. Ni 2p and Pt 4f XPS spectra of catalysts Ni and $Ni_x@Pt_{1-x}$

Therefore, the highest catalytic activity is obtained with the lowest amount of Pt in the shell, in agreement with the calculated results of the maximum effect of the core when a monolayer of platinum is interacting with the Ni core, while higher amounts of Pt result in a slightly lower catalytic activity, resembling the results of an almost null effect of the core with the second and totally null after the third monolayer of Pt in total agreement with the results of the slab approach. However, the energetic differences in oxygen E_{ads} between modelling the strained and non-strained slab systems, imposed a limit on the usefulness of this approach, since the results are model-dependent. Even though the results are qualitatively similar, the

fundamental differences between the models lead to uncertainty on the predictions which make mandatory the implementation of better models to represent the core-shell structure.

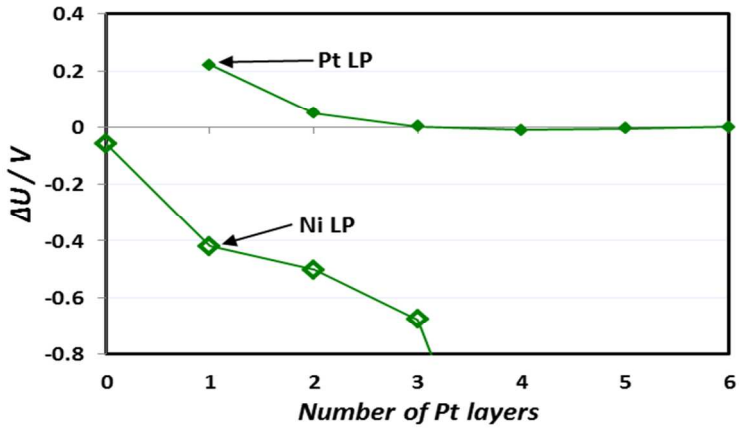

Figure 4. Core/shell Ni@Pt stability properties for the two slab models: dissolution potential shift as a function of the number of Pt layers for Pt and Ni LP.

The differences in both models are more drastic analyzing the dissolution potential shift for surface atoms (Figure 4). Ma and Balbuena[28,49] developed a method to evaluate the stability towards dissolution of surfaces by analyzing the dissolution potential shift caused by removal of an atom from the surface (ΔU). This quantity indicates the easiness to remove one Pt surface atom in a specific system in comparison to the removal of a Pt atom from the pure Pt surface. For a positive shift on the dissolution potential the system is more stable than pure Pt while the opposite indicates a less stable system. Our results for Ni@Pt modelled on the slab approach indicate that in the case of the non-strained system (Pt LP) five, four, and three Pt layers have the same dissolution potential as pure platinum. In other words, beyond the second layer on the shell the core has a null effect; however, the Pt monolayer on the Ni core is indeed more stable towards dissolution than pure Pt. On the contrary, when the shell layers are strained ΔU is negative, becoming even more negative as more layers are added. Therefore, both models predict opposite stability trends which make them totally useless as predictive methods.

The limitations imposed by the periodic slab system lead to extreme results; however a modified procedure allowing relaxation of the interface could lead to a more tolerant system in which the stability properties are better represented. In additional simulations, the strained slabs used in the previous section were allowed to relax in the xy direction. By doing so we are relaxing the interface but also, changing the properties of the core (represented by the bottom layers of the slab); however, it is important to analyze such an intermediate situation. The relaxation of the interface leads to different metal-metal distances (M-M) on the surface; those differences are depicted in Figure 5a. For the systems with a higher amount of Ni the initial structure presents M-M distances of Ni LP, after relaxation the final M-M distance is slightly larger than to those found on pure Ni; on the other hand, for the higher amount of Pt the initial structure has M-M distances of Pt LP, and after relaxation it leads to shorter distances than in Pt after interface relaxation. However, for an intermediate value, the relaxations with Ni or Pt LP lead to almost the same M-M distances.

Another set of computational experiments was also performed in which we fixed the amount of layers in the core (4 layers) while adding one by one Pt layers. In this case, for one Pt layer (as the proportion of Ni to Pt layers is lower) the M-M distance is slightly larger than the one obtained for a Pt monolayer on the 6-layer slab. Similar behavior stands for three and four layers of Pt, leading to shorter M-M distances because of the higher amount of Ni. The corresponding dissolution potential shift of all the relaxed systems is depicted on Figure 5b; the same scale as in Figure 4 is used to highlight the changes. Differently than the strained systems, the relaxed ones present small changes in ΔU, the systems with a higher amount of Pt present a value of ΔU close to 0 but positive, while those with higher amount of Ni (still very similar M-M distances of pure Ni) present negative ΔU, in all cases suggestion a similar stability as in the case of a pure Pt slab. For the systems with a fixed amount of Ni on the core the first layer presents a slightly positive ΔU but it quickly goes to negative for the cases of two and three Pt layers; however, for the fourth layer as in the strained system it approaches again to an almost zero ΔU value. Even though, the model is less constrained the results are still system-dependent and not conclusive since the planarity of the surface might be interfering. In summary, the slab approach could lead to very different results depending on the assumptions used to model the system.

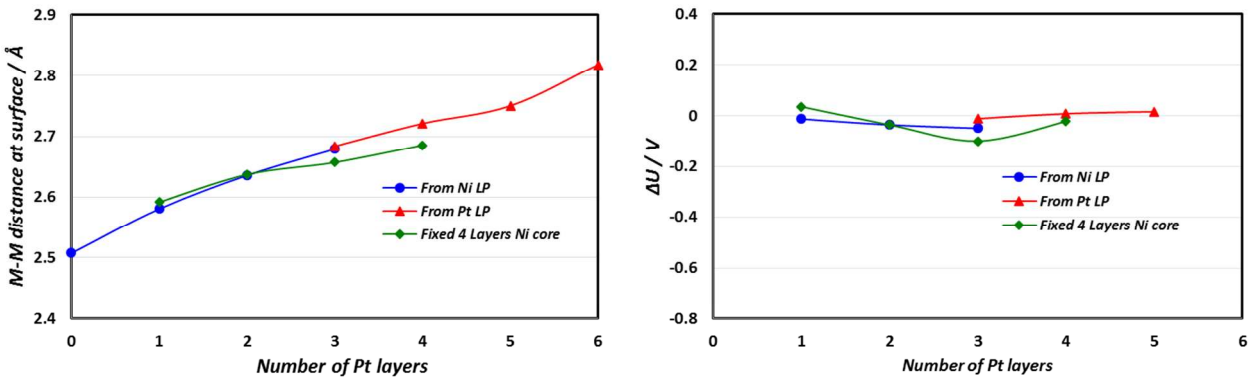

Figure 5. Comparison of geometric and stability properties of the relaxed slab systems (see text for details). a) M-M distance at the surface, b) Dissolution potential shift of Pt on the surface.

In order to find out what are the sources of error in the slab approach, a new set of cluster simulations were performed with nanoparticles having 13 to 260 atoms in size; the largest cluster having a diameter slightly larger than 2 nm. The geometry of the Pt_{13} cluster is icosahedral with one atom in the center, this is the smallest core@shell nanoparticle possible, previous reports have used this small cluster to model core@shell catalysts [50,51]. On the other hand, in order to get the (100) and (111) facets of real nanoparticles, from Pt_{38} to Pt_{260} truncated cuboctahedra were constructed adding layer by layer to a 6 atom Pt cluster with O_h symmetry. This structural evolution (from icosahedral to fcc-like clusters as the cluster size increases) has been suggested on the basis of DFT calculations[52] that examined three different growth pathways and the approximate sizes where transitions between these structures may occur. Although simulated annealing approaches have been used for exploring potential energy minima for the clusters [53,54], we have not used this approach here. Figure 6 depicts the geometry of the clusters highlighting the (111) and (100) facets. For the smallest cluster, only (111) facets composed of three atoms are found, for the larger clusters both (111) and (100) planes are present. For the construction of core@shell nanoparticles the center of the Pt nanoparticle was replaced with Ni atoms and re-optimized. All clusters include at

least one atom as core while the number of layers of Pt in the shell was varied from 1 to 3 when possible. For the Pt_{13} and Pt_{38} nanoparticles only one layer of Pt in the shell is possible; in those cases the cluster core is formed by one atom and six atoms, respectively. For Pt_{116} an extra layer was added over the Pt_{38} cluster; therefore two core/shell nanoparticles are possible, one with a monolayer shell and another with a two-layer Pt shell. Finally for Pt_{260} a monolayer, bilayer and three-layer of Pt shell are possible.

Two geometric properties are analyzed for the nanoparticles: diameter and planarity of the (111) facets. The size of the nanoparticles varies from 0.5 nm in Pt_{13} to ~2.0 nm in the largest nanoparticles, modelling bigger nanoparticles is out of the computational capabilities in most current research facilities. The core-shell nanoparticles are always smaller than their pure Pt counterpart as a consequence of the smaller Ni size (shorter Ni-Ni distances) but also because of the strong interaction between Pt and Ni. Due to the strong interaction, the planarity of the facets also changes. In the Pt clusters, the central part of any facet is more separated from the core than the edge atoms are, but in the Ni@Pt clusters the separation is shorter. The angle indicated in Figure 5 was measured between three atoms: one in the edge of the facet, another in the middle and a third in the opposite edge. As the cluster size is raised the planarity is enhanced in both core@shell and Pt clusters; however, at any size the Ni@Pt cluster facets are more planar than on the Pt ones.

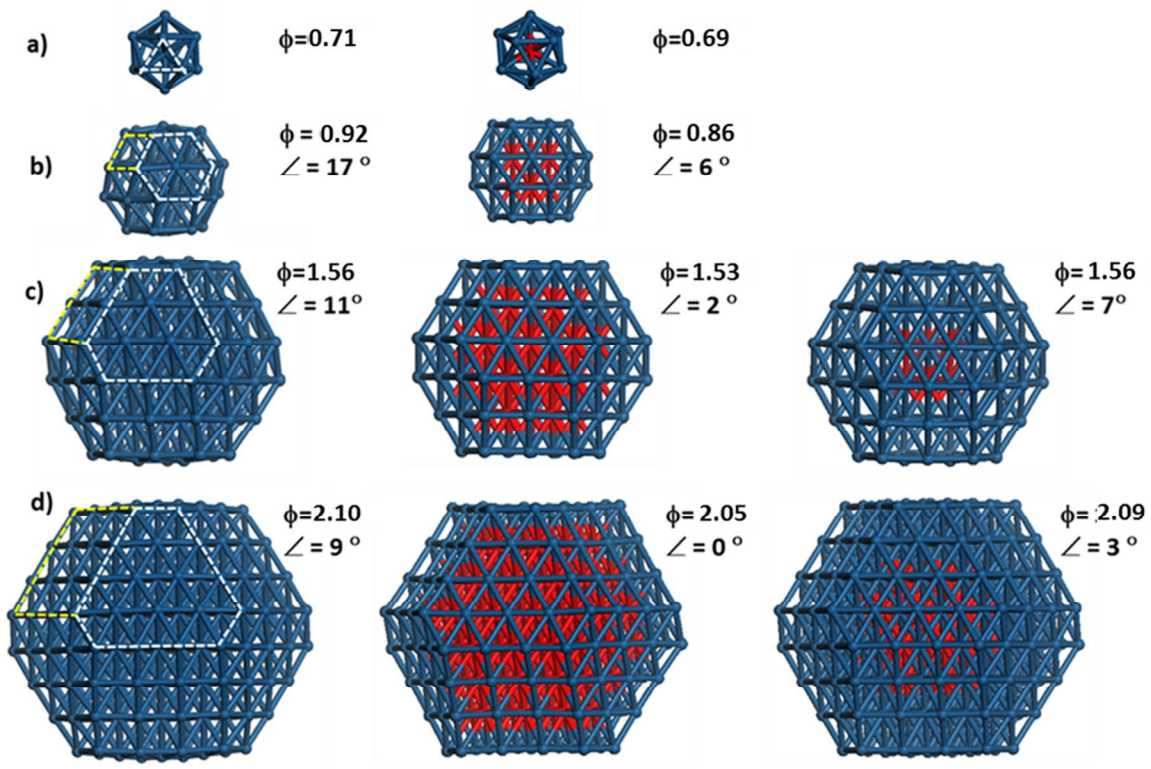

Figure 6. Metallic clusters of pure Pt and Ni@Pt with different number of layers a) Pt_{13}, $Pt_{12}Ni_1$, b) Pt_{38}, $Pt_{32}Ni_6$, c) Pt_{116}, $Pt_{78}Ni_{38}$, $Pt_{110}Ni_6$, d) Pt_{260}, $Pt_{144}Ni_{116}$, $Pt_{222}Ni_{38}$. Blue and red spheres represent Pt and Ni atoms respectively. The angle is an indicator of the planarity of the facet (see text). The diameter ϕ is given in nm taking into account the atomic diameter.

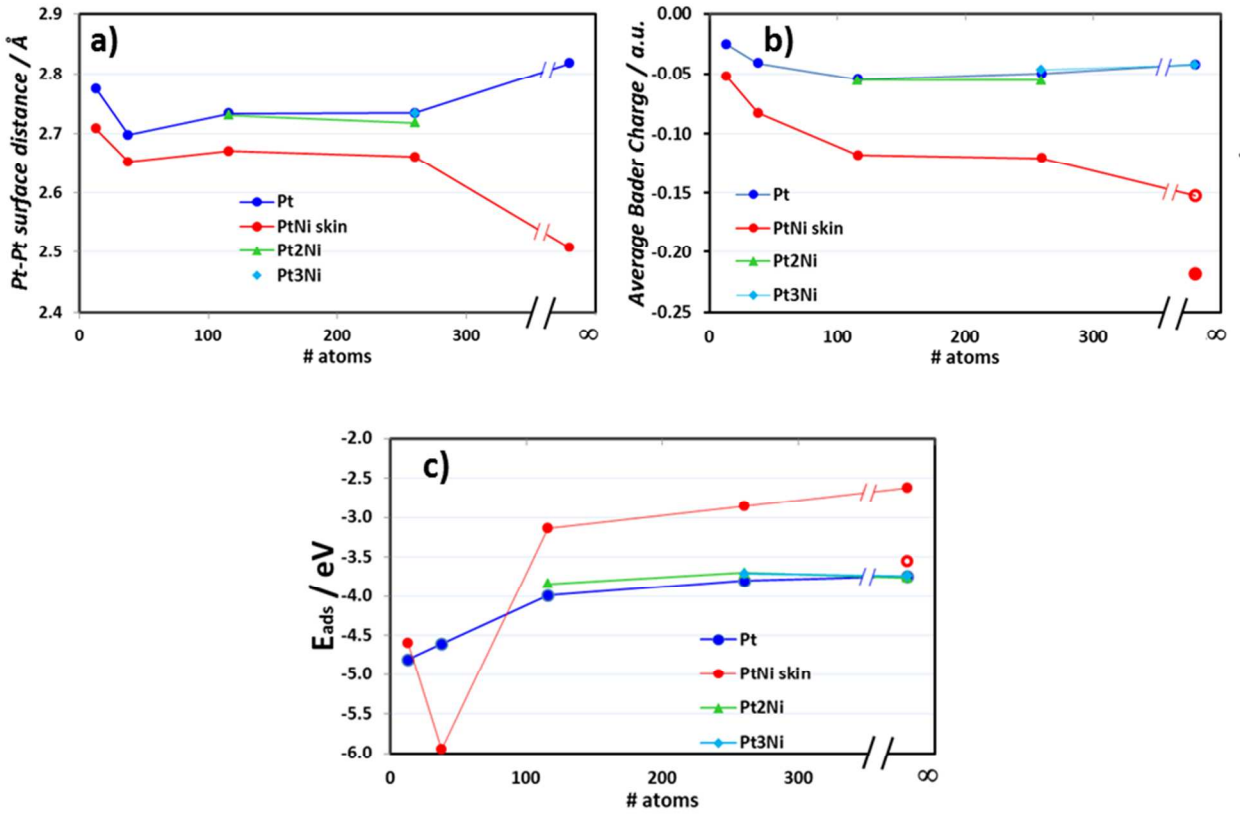

Figure 7. Cluster geometric and energetic properties as function of size and number of layers in the shell. a) Pt-Pt distance in the (111) facet, b) Average Bader charge of Pt atoms in the (111) facet, and c) Oxygen adsorption energy (E_{ads}) in fcc sites of the (111) facet. Values calculated with the slab approach with Pt LP and Ni LP are depicted with open and close circles respectively at the infinite size limit.

The differences in size and shape are expected to have an effect on the catalytic properties and nanoparticle stability that could be fundamentally different than those observed in the slab approach. The Pt-Pt distance on the (111) facets in the Pt nanoparticle serves to quantify the differences with the slab approach. For very small size Pt clusters the Pt-Pt distance takes values from 2.7 to 2.8 Å, however for larger nanoparticles the distance reaches a constant value of 2.73 Å (Fig 7a). Although for nanoparticles larger than 2.5 nm it would be expected that the Pt-Pt distance reaches the bulk limit (2.82 Å), Figure 7a shows a value smaller than in the bulk. However the same size leads to a very similar Bader charge on the Pt atoms than that obtained with the slab approach (Fig 7b blue line) and also to a very similar oxygen adsorption energy than in the slab calculation (Fig. 7c blue line). The result is surprising since one fundamental property such as the Pt-Pt distance is different than that predicted by the slab calculation but electronic properties (Bader charges, adsorption energies) are similar to those of the periodic (bulk surface) results. On the other hand for core@shell nanoparticles of any given size with one layer of Pt (PtNi-skin) the Pt-Pt distance on the surface is shorter than the Pt nanoparticles of the same size. For the small NPs large fluctuations are observed on the adsorption energies and also in the Pt-Pt distance reaching a constant value after 116 atoms. However, the constant value reached for Pt-Pt distances is not that of the

bulk Pt neither that of Ni bulk, indicating that the assumption on the slab simulation of either approach (Ni or Pt LP) is fundamentally incorrect especially for structural properties. For all the structures with a higher number of Pt layers on the shell the effect of the core is only appreciable on the first layer, on the second layer a slight effect on the Pt-Pt distance, Bader charges and E_{ads} can be seen but beyond the third layer the changes are negligible leading to the same adsorption energy than in pure Pt. These results agree qualitatively with those obtained on the slab approach, for a second and third layer the effect of the core is nullified.

The experimental analysis provides new insights into the structure of the nanoparticles. In order to determine the changes occurring on the lattice parameter of the samples of Ni@Pt, X-ray diffraction patterns with Rietveld refinement were obtained of the as-prepared catalysts. The XRD patterns for $Ni_x@Pt_{100-x}$ samples depicted well separated peaks for Ni and Pt elements, which strongly suggest well segregated phases[55]. Another possibility is to have separated Ni and Pt nanoparticles; however, voltammetric studies show that the oxidation of Ni occurs at ~ 0.4 V (ENH). Therefore the pure Ni core presents an oxidation peak at this potential, while only the Ni@Pt nanoparticles with the lowest amount of Pt presents a small oxidation peak indicating an incomplete Pt monolayer (Supplementary information Figure S2). Therefore, for all the other samples, the presence of pure Ni nanoparticles after the core shell formation is ruled out. Considering different factors which might influence a specific structural conformation (i.e. interaction energies between components, surface energies of bulk elements, charge transfer etc.), in our case, besides the possible influence from the factors outlined above, we propose that Pt enrichment on the surface is promoted by the synthesis pathway. Overall, for the $Ni_x@Pt_{100-x}$ catalysts the diffraction peaks associated with the Pt phase were shifted to higher angles depending on Ni:Pt ratio (see Supplementary Information Figure S3 and Table S2). This feature was explained by a contraction on the Pt lattice parameters: 3.798, 3.917 and 3.845 Å for 18, 38, and 70 Pt wt. % respectively, which were shorter than the average of the individual lattice constant of Pt for Pt/C sample (3.924 Å)[36]. The simulations using the cluster approach for different number of layers in the shell indicate almost an insignificant effect for thicker shells. The properties like the Pt-Pt distance on the nanoparticle surface, charge of surface atoms and in consequence on the oxygen adsorption energy for two and three monolayers of Pt are not affected by the core. The results are in line with the XRD analyses in which only for the lowest amount of Pt the changes in Pt lattice contraction resultant from the core are evident. When the Pt amount increases, a Pt lattice relaxation occurs demonstrated by the larger Pt lattice parameters. Therefore, both experimental and theoretical simulations on the cluster approach indicate that a kind of "*radial outward relaxation*" occurs when the number of Pt monolayers increases, this type of relaxation is impossible to be observed on the simulations with fixed lattice parameters used with the slab approach.

For the PtNi skin a series of different values are observed on the simulations for the larger cluster, 1) the Pt-Pt distance is an intermediate between Pt and Ni LP, 2) the Bader charge of the Pt atoms is lower than any value obtained from the slabs calculations; however, 3) the oxygen adsorption energy in large nanoparticles is very similar to that obtained in the slab approach on the strained system while the non-strained system does underestimate the changes in adsorption energy. This behavior indicates that the contributions from atomic charges and bond lengths on the surface of a nanoparticle determine the oxygen adsorption; while in the slab approach only one value is well represented, in the nanoparticle the contribution from all of them leads to the correct O-Pt interaction. The trends for oxygen adsorption energy depicted in Figure 7c indicate weaker adsorption energy of oxygen as the cluster size is increased on PtNi skin, reach-

ing an almost constant value for larger nanoparticles in both Ni@Pt and Pt; except for the cluster of 38 atoms in which reconstruction of the cluster occurs, in agreement with other studies of small clusters [56].

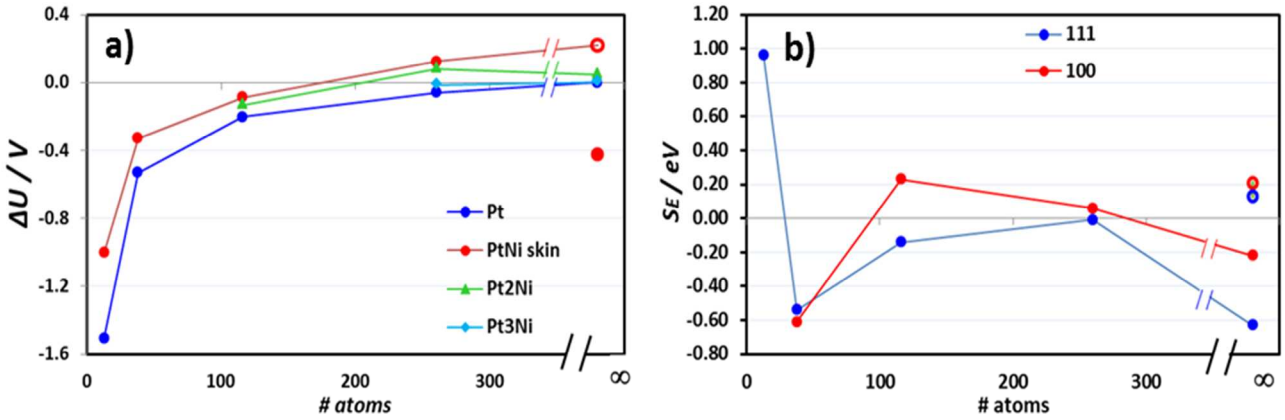

Figure 8. Stability properties of the nanoparticles: a) Dissolution potential shift as function of size and number of Pt layers in the shell and b) Segregation energy of the Ni atoms to the surface in the 111 a 100 facets as function of size (Slab values of the for Ni and Pt LP are depicted as close and open symbols respectively at the infinite limit)

For the stability of the nanoparticles, the dissolution potential shift was again calculated with reference to the value of the pure Pt surface. It is observed that at the same size the dissolution potential of the PtNi skin is more positive than that of the Pt nanoparticle indicating that whenever a Pt layer is interacting at least with one Ni atom the system becomes more stable against dissolution. Thus, a more difficult oxidation process takes place for the Pt atoms on the surface; moreover the 2-layer Pt system is still a little bit more stable while the 3-layered Pt is almost identical to that of pure Pt. Nevertheless, for smaller particles of Pt and PtNi skin the oxidation is easier than the oxidation of the bulk system, as it is expected due to their low cohesive energy which makes them very reactive. For the larger Pt nanoparticles the dissolution shift is still negative in comparison to the bulk system as expected for a nanoparticle in comparison to the bulk surface; however the PtNi skin presents at this size already a positive shift in dissolution potential which resembles the value obtained in the slab calculation when the slab is not constrained to the Ni LP. On the other hand, the negative value obtained on the slab approach of the strained system is totally overestimated. For a higher number of layers the results are very similar to those reported in the slab approach with the non-strained system: intermediate values between the pure Pt and PtNi skin, with two Pt layers being more similar to the PtNi skin and the three-layer Pt more similar to those of the pure Pt nanoparticle. Therefore, a basic parameter as the metal-metal distance at the interface of a core@shell structure is of primordial importance in order to truly represent the changes in reactivity and stability of a real nanoparticle but also the importance of the null constrain during oxygen adsorption and removal of surface atoms.

Another fundamental factor on the stability and durability of the materials is the segregation of components towards the surface. The external surface could be more stable against dissolution; but, if segregation of less noble metal atoms to the surface occurs, their dissolution is possible. Segregation energy should be also a function of the model used to represent the nanoparticle. For the segregation energy analysis, the two facets of the nanoparticle (depicted in Figure 6) were analyzed. The segregation energy

was obtained by calculating the difference in energy between the original system and that in which one Ni atom in the subsurface by one Pt on the surface is exchanged. If the segregation energy values are negative, segregation takes place, while antisegregation is suggested by positive energies. For smaller nanoparticles the results present high variations related to the different geometries and coordination numbers; however, for larger nanoparticles as the facets become more similar to an extended surface, a clear trend is observed. For the (100) facets the segregation energy is positive (antisegregation) but diminishes as the cluster grows. In contrast, for the (111) the segregation energy is negative (allowed process) becoming less negative as the cluster grows. It should be noted that the negative segregation energy in the (111) facet is almost zero while the positive is very small, which lead us to conclude that the segregation might be small at larger cluster sizes. The slab approach predicts that the strained system has negative segregation energy in the (111) and (100) facets but for the non-strained system presents the opposite behavior for both facets. Therefore, the slab approach again is an incomplete model that does not represent well the behavior of a real nanoparticle. The calculations here presented were carried out in vacuum implying that the nanoparticles are stable in non-oxidizing conditions; however, the scenario could change when oxygen and acidic species and an electrochemical potential are present.

We have performed preliminary stability tests with promising results suggesting good stability for the $Ni_8@Pt_2/C$ catalysts. After 5k cycles, loss of activity was not detected respect to the initial. Monitoring the changes on surface area by CO stripping every 1k cycles, revealed surface increment during the first 1k cycles. Then a steady decrease and a final surface loss of ~ 20 %, considering the maximum area at 1k, were observed [57]. The results are in agreement with the simulations of core@shell performed with the cluster approach in which the oxidation of Pt is diminished and the segregation of Ni components is small. This is in contrast to the results from the slab approach in which the extreme strain imposed by the Ni core lead to a prediction of low stability. Therefore, the influence of oxygen concentration, continuous polarization and formation of other species, for instance hydrogen peroxide, are probably the cause of the degradation of the catalyst but not the simple fact of the formation of the core@shell structure and the strain imposed by Ni. Analysis of the degradation including several factors as those aforementioned is in progress and will be published elsewhere.

Conclusions

Modelling a core shell nanoparticle with a slab approach could be useful to represent some specific properties; however, depending on the geometric parameters of the core the results can be less accurate and have less predictive power. For Ni@Pt, modelling the surface layer strained to the geometric parameters of the core represents well the changes observed in a ~2nm nanoparticle but the same model predicts results of surface stability in total disagreement with the results obtained for the ~2nm nanoparticle. Another limitation of the slab approach is the lack of capability to represent the surface expansion observed by XRD and nanoparticle simulations of the different metal-metal distances on the interface that are different to both core and shell components. Despite allowing expansion on the slab model the predictions are still far from reality. Moreover, the radial outward relaxation is only observed on the nanoparticle simulation and verified by XRD and Rietveld analysis. The most important finding of this study is the demonstration that by the proper method of synthesis Ni@Pt nanoparticles are stable at least in non-oxidizing conditions as predicted by cluster simulations in which the Pt layer is not totally strained to the geometric parameters of Ni but the effect of the strong interaction with nickel shifts the oxidation potential to slightly more positive values. This study opens up the route for the implementation of better models in order to

represent correctly the nanoparticle properties we suggest at least that the real metal-metal distances at the interface can be evaluated first by a cluster model and then applied to the slab or totally shift to > 2nm nanoparticles as a model.

Acknowledgements

This research project was possible thanks to the support of CONACYT-TAMU project 2013-016 and CONACYT postdoctoral fellowship to GRS. Computational resources from Texas A&M supercomputing facilities, Texas Advanced Computing Center, and Brazos cluster at Texas A&M are gratefully acknowledged.

References

(1) Murthy, S. S.; Kumar, E. A.: *Applied Thermal Engineering* 2014, **72**, 176-189.
(2) Dresselhaus, M. S.; Thomas, I. L.: *Nature* 2001, **414**, 332-337.
(3) Garcia-Mota, M.; Vojvodic, A.; Metiu, H.; Man, I. C.; Su, H. Y.; Rossmeisl, J.; Norskov, J. K.: *Chemcatchem* 2011, **3**, 1607-1611.
(4) Gonzalez-Huerta, R. G.; Ramos-Sanchez, G.; Balbuena, P. B.: *Journal of Power Sources* 2014, **268**, 69-76.
(5) Yu, X. W.; Ye, S. Y.: *J. Power Sources* 2007, **172**, 145-154.
(6) Peng, Z. M.; Yang, H.: *Nano Today* 2009, **4**, 143-164.
(7) Zhang, J.; Vukmirovic, M. B.; Sasaki, K.; Nilekar, A. U.; Mavrikakis, M.; Adzic, R. R.: *Journal of the American Chemical Society* 2005, **127**, 12480-12481.
(8) Vukmirovic, M. B.; Zhang, J.; Sasaki, K.; Nilekar, A. U.; Uribe, F.; Mavrikakis, M.; Adzic, R. R.: *Electrochimica Acta* 2007, **52**, 2257-2263.
(9) Greeley, J.; Norskov, J. K.; Mavrikakis, M.: *Ann. Rev. Phys. Chem.* 2002, **53**, 319-348.
(10) Greeley, J.; Mavrikakis, M.: *Nat. Mat.* 2004, **3**, 810-815.
(11) Kitchin, J. R.; Norskov, J. K.; Barteau, M. A.; Chen, J. G.: *J. Chem. Phys.* 2004, **120**, 10240-10246.
(12) Kitchin, J. R.; Norskov, J. K.; Barteau, M. A.; Chen, J. G.: *Phys. Rev. Lett.* 2004, **93**, 156801.
(13) Kitchin, J. R.; Norskov, J. K.; Barteau, M. A.; Chen, J. G.: *J. Chem. Phys.* 2004, **120**, 10240-10246.
(14) Menning, C. A.; Chen, J. G.: *J. Chem. Phys.* 2008, **128**, 164703.
(15) Yu, P.; Pemberton, M.; Plasse, P.: *J. Power Sources* 2005, **144**, 11-20.
(16) Dubau, L.; Castanheira, L.; Maillard, F.; Chatenet, M.; Lottin, O.; Maranzana, G.; Dillet, J.; Lamibrac, A.; Perrin, J.-C.; Moukheiber, E.; ElKaddouri, A.; De Moor, G.; Bas, C.; Flandin, L.; Caque, N.: *Wiley Interdisciplinary Reviews-Energy and Environment* 2014, **3**, 540-560.
(17) Xin, H.; Holewinski, A.; Linic, S.: *Acs Catalysis* 2012, **2**, 12-16.
(18) Nilekar, A. U.; Mavrikakis, M.: *Surf. Sci.* 2008, **602**, L89-L94.
(19) Zhang, X.; Yu, S.; Zheng, W.; Liu, P.: *Physical Chemistry Chemical Physics* 2014, **16**, 16615-16622.
(20) Zhang, J.; Vukmirovic, M. B.; Xu, Y.; Mavrikakis, M.; Adzic, R. R.: *Angew. Chem. Int. Ed.* 2005, **44**, 2132-2135.
(21) Xu, Y.; Ruban, A. V.; Mavrikakis, M.: *J. Am. Chem. Soc.* 2004, **126**, 4717-4725.
(22) Norskov, J. K.; Rossmeisl, J.; Logadottir, A.; Lindqvist, L.; Kitchin, J. R.; Bligaard, T.; Jonsson, H.: *J. Phys. Chem. B* 2004, **108**, 17886-17892.
(23) Kitchin, J. R.; Reuter, K.; Scheffler, M.: *Phys. Rev. B* 2008, **77**, 075437.
(24) Shin, K.; Kim, D. H.; Yeo, S. C.; Lee, H. M.: *Catalysis Today* 2012, **185**, 94-98.

(25) Yancey, D. F.; Zhang, L.; Crooks, R. M.; Henkelman, G.: *Chem. Sci.* 2012, **3**, 1033-1040.
(26) Cheng, D.; Qiu, X.; Yu, H.: *Physical Chemistry Chemical Physics* 2014, **16**, 20377-20381.
(27) Skoplyak, O.; Menning, C. A.; Barteau, M. A.; Chen, J. G.: *Journal of Chemical Physics* 2007, **127**.
(28) Ramirez-Caballero, G. E.; Ma, Y.; Callejas-Tovar, R.; Balbuena, P. B.: *Phys. Chem. Chem. Phys.* 2010, **12**, 2209-2218.
(29) Wang, C.; Chi, M.; Li, D.; Strmcnik, D.; van der Vliet, D.; Wang, G.; Komanicky, V.; Chang, K.-C.; Paulikas, A. P.; Tripkovic, D.; Pearson, J.; More, K. L.; Markovic, N. M.; Stamenkovic, V. R.: *Journal of the American Chemical Society* 2011, **133**, 14396-14403.
(30) Hasche, F.; Oezaslan, M.; Strasser, P.: *Journal of the Electrochemical Society* 2012, **159**, B25-B34.
(31) Kuttiyiel, K. A.; Sasaki, K.; Su, D.; Vukmirovic, M. B.; Marinkovic, N. S.; Adzic, R. R.: *Electrochimica Acta* 2013, **110**, 267-272.
(32) Kresse, G.; Hafner, J.: *Physical Review B: Condensed Matter and Materials Physics* 1993, **47**, 558-61.
(33) Kresse, G.; Furthmuller, J.: *Phys. Rev. B* 1996, **54**, 11169-11186.
(34) Blochl, P. E.: *Phys. Rev. B* 1994, **50**, 17953-17979.
(35) Hammer, B.; Hansen, L. B.; Norskov, J. K.: *Phys. Rev. B* 1999, **59**, 7413-7421.
(36) Godinez-Salomon, F.; Hallen-Lopez, M.; Solorza-Feria, O.: *Int. J. Hydrog. Energy* 2012, **37**, 14902-14910.
(37) Garsany, Y.; Baturina, O. A.; Swider-Lyons, K. E.; Kocha, S. S.: *Anal. Chem.* 2010, **82**, 6321-6328.
(38) Stamenkovic, V.; Mun, B. S.; Mayrhofer, K. J. J.; Ross, P. N.; Markovic, N. M.; Rossmeisl, J.; Greeley, J.; Norskov, J. K.: *Angewandte Chemie, International Edition* 2006, **45**, 2897-2901.
(39) Greeley, J.; Stephens, I. E. L.; Bondarenko, A. S.; Johansson, T. P.; Hansen, H. A.; Jaramillo, T. F.; Rossmeisl, J.; Chorkendorff, I.; Norskov, J. K.: *Nat. Chem.* 2009, **1**, 552-556.
(40) Hansen, H. A.; Rossmeisl, J.; Norskov, J. K.: *Physical Chemistry Chemical Physics* 2008, **10**, 3722-3730.
(41) Karlberg, G. S.: *Phys. Rev. B* 2006, **74**, 153414.
(42) Jacob, T.; Muller, R. P.; W. A. Goddard, I.: *J. Phys. Chem. B* 2003, **107**, 9465-9476.
(43) Jacob, T.; Goddard, W. A.: *Journal of Physical Chemistry B* 2004, **108**, 8311-8323.
(44) Biesinger, M. C.; Payne, B. P.; Grosvenor, A. P.; Lau, L. W. M.; Gerson, A. R.; Smart, R. S. C.: *Applied Surface Science* 2011, **257**, 2717-2730.
(45) Balbuena, P. B.; Callejas-Tovar, R.; Hirunsit, P.; de la Hoz, J. M. M.; Ma, Y.; Ramirez-Caballero, G. E.: *Top. Catal.* 2012, **55**, 322-335.
(46) Gan, L.; Heggen, M.; Rudi, S.; Strasser, P.: *Nano Letters* 2012, **12**, 5423-5430.
(47) Chung, Y.-H.; Chung, D. Y.; Jung, N.; Park, H. Y.; Yoo, S. J.; Jang, J. H.; Sung, Y.-E.: *Journal of Physical Chemistry C* 2014, **118**, 9939-9945.
(48) Callejas-Tovar, R.; Diaz, C. A.; de la Hoz, J. M. M.; Balbuena, P. B.: *Electrochimica Acta* 2013, **101**, 326-333.
(49) Ma, Y.; Balbuena, P. B.: *J. Phys. Chem. C* 2008, **112**, 14520-14528.
(50) Apra, E.; Fortunelli, A.: *Journal of Physical Chemistry A* 2003, **107**, 2934-2942.
(51) Zhao, F.; Liu, C.; Wang, P.; Huang, S.; Tian, H.: *J. Alloy. Compd.* 2013, **577**, 669-676.
(52) Nie, A. H.; Wu, J. P.; Zhou, C. G.; Yao, S. J.; Forrey, R. C.; Cheng, H. S.: *Int. J. Quantum Chem.* 2007, **107**, 219-224.
(53) Ojwang, J. G. O.; van Santen, R.; Kramer, G. J.; van Duin, A. C. T.; Goddard, W. A.: *J. Chem. Phys.* 2008, **129**.

(54) Rogan, J.; Garcia, G.; Loyola, C.; Orellana, W.; Ramirez, R.; Kiwi, M.: *J. Chem. Phys.* 2006, **125**.

(55) Wu, Q.; Eriksen, W. L.; Duchstein, L. D. L.; Christensen, J. M.; Damsgaard, C. D.; Wagner, J. B.; Temel, B.; Grunwaldt, J.-D.; Jensen, A. D.: *Catalysis Science & Technology* 2014, **4**, 378-386.

(56) Oemry, F.; Nakanishi, H.; Kasai, H.; Maekawa, H.; Osumi, K.; Sato, K.: *J. Alloy. Compd.* 2014, **594**, 93-101.

(57) Ramos-Sanchez, G.; Godinez-Salomon, F.; Solorza-Feria, O.; Balbuena, P. B.: Activity and Durability of PEFCs Alloy Core-Shell Catalysts: Role of Surface Oxidation. In *Advances in Science and Technology. 6th forum on New Materials - Part A*; Vincenzini, P., Ed., 2014; Vol. 93; pp 31-40.

Table of Contents Entry

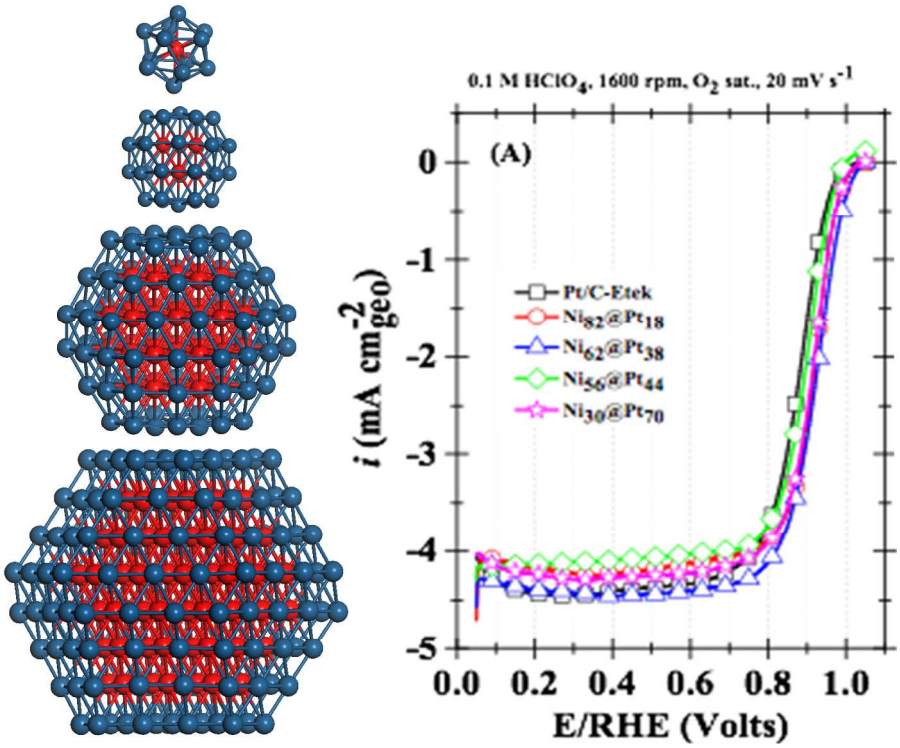

Core-shell nanoparticle properties strongly dependent on cluster size and composition